Wave Feedforward Control for Large Floating Wind Turbines

Hegazy, Amr; Naaijen, Peter; Van Wingerden, Jan Willem

DOI
10.1109/CCTA54093.2023.10252529

Publication date
2023

Document Version
Final published version

Published in
Proceedings of the 2023 IEEE Conference on Control Technology and Applications, CCTA 2023

2023 IEEE Conference on Control Technology and Applications (CCTA)
August 16-18, 2023. Bridgetown, Barbados

Wave Feedforward Control for Large Floating Wind Turbines*

Amr Hegazy[1], Peter Naaijen[2] and Jan-Willem van Wingerden[1]

2023 IEEE Conference on Control Technology and Applications (CCTA) | 979-8-3503-3544-6/23/$31.00 ©2023 IEEE | DOI: 10.1109/CCTA54093.2023.10252529

***Abstract*— Floating wind energy has attracted substantial interest since it enables the deployment of renewable wind energy in deeper waters. However, floating wind turbines are subjected to disturbances, predominantly from turbulence in the wind and waves hitting the platform. Wave disturbances cause undesired oscillations in speed and increase structural loading. This paper focuses on mitigating these disturbance effects with feedforward control using knowledge of the incoming wavefield. The control problem is formulated in an $\mathcal{H}_\infty$ optimization framework designing two wave feedforward controllers: one to reduce rotor speed oscillations, and the other one to minimize the platform pitch motion. Mid-fidelity time-domain simulations demonstrate the improved performance of the proposed control algorithm regarding wave disturbance mitigation at the cost of higher actuator duty.**

I. INTRODUCTION

Driven by the European Commission's ambition of becoming a climate-neutral continent by 2050, wind energy is the technology expected to provide the largest contribution to the EU renewable energy targets [1].

Apart from these advantages, offshore wind energy is even more challenging due to the rough environmental operating conditions. Especially, with waves added to the disturbances affecting the wind turbine, and exerting extra structural loading on top of the loads due to wind turbulence. Waves contribute to the fatigue loads experienced by the floating offshore wind turbines (FOWTs). From a control perspective, FOWTs are harder to control than their onshore counterpart. That is due to the extra dynamics introduced by the floating platform, and the well-known negative damping instability forcing a reduction in the bandwidth of the feedback pitch controller below the platform pitch eigenfrequency [2]. Consequently, the control authority of the blade pitch feedback controller against errors occurring due to disturbances such as wind and waves becomes limited. Regarding wind turbulence, LiDAR FeedForward (FF) control, which is based on providing a preview of the upstream wind field to be included in the turbine controller, has been the main focus of feedforward control in wind turbines, as it proved to reduce fatigue loads and power excursions effectively [3], [4].

Wave FF control strategy resembles LiDAR FF control, as in the case of wave FF, a preview of the wave height/loads is also required to be exploited within the turbine controller. In this regard, several technologies are available to measure the surface wave elevation as wave buoys, radars, or satellites. The radar technology, in particular, is attractive because of its capability in scanning large areas at further distances [5]. Radar images of the wave field can then be used to obtain predictions of the surface wave elevation as in [6]. Wave FF, however, is not discussed in the literature as thoroughly yet. Only a few studies investigated the subject as in [7] where a Non-linear Model Predictive Control (NMPC) strategy was developed, considering perfect wind/wave preview, demonstrating promising improvement over the baseline feedback controller with regard to blade loads. In [8], an effective deterministic finite-horizon LQR controller was designed, exploiting a real-time forecast of the wave loads, to reduce tower-base fore-aft (FA) bending moment, and achieved assorted results. An inversion-based wave FF controller was developed in [5], [9] utilizing a preview of the incoming wave elevation, where the FF controller was added to the standard feedback (FB) controller to refine power quality by reducing the rotor speed fluctuations caused by waves. The controller effectively alleviates the effects of the wave disturbance, decreasing rotor speed excursions with a positive side-effect of lowering the fatigue loads for the Low-Speed Shaft (LSS) and blades. However, the model-based inverted

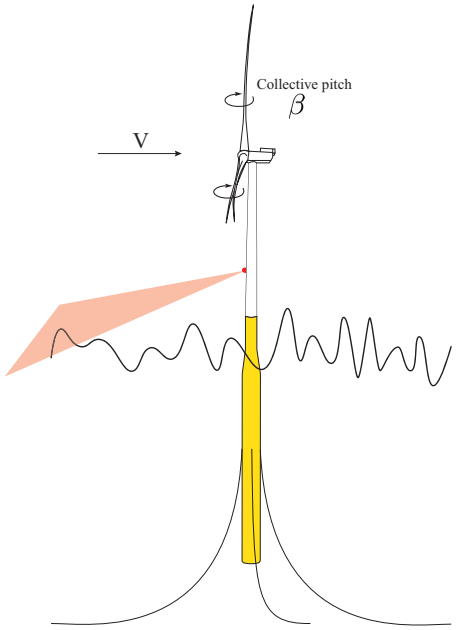

Fig. 1. Schematic of the wave feedforward control strategy. The feedforward control action is based on the wave elevation measured by a radar upstream of the wind turbine. This measurement is used to obtain a preview of the wave excitation forces at the floating platform ahead of time, which is the input to the wave feedforward controller.

*This project is part of the FLOATECH project. The research presented in this paper has received funding from the European Union's Horizon 2020 research and innovation programme under grant agreement No. 101007142.

[1]Delft Center for Systems and Control, Delft University of Technology, Delft, 2628 CD, The Netherlands a.r.hegazy@tudelft.nl

[2]Maritime and Transport Technology, Delft University of Technology, Delft, 2628 CD, The Netherlands

FF controller in [5], [9] only considers a few degrees of freedom corresponding to the global dynamics of the FOWT, which means that it lacks extra modes, in addition to other missing elements, namely the non-minimum phase behavior arising from the Right-Half Plane Zeros (RHPZs) in the plant model. In this paper, two wave FF controllers are developed; one for alleviating the rotor speed oscillations for power regulation (FF-ω), and the other for mitigating the platform pitch motion for load minimization (FF-θ_p).

Unlike the model-based control used in [5], [9] for the control synthesis, the data-driven control approach can capture the unknown dynamics unconsidered in the model-based. Therefore, it was adopted in this paper using the Predictor-Based Subspace Identification (PBSID$_{opt}$) algorithm [10]. The main contributions of this paper are threefold:

- A linear model of a FOWT, with blade pitch control input and wave excitation forces as disturbance input, is identified using PBSID$_{opt}$ method.
- Two wave forward controllers are synthesized for the objectives of power regulation and load mitigation.
- The performance of the developed controllers is then assessed in the mid-fidelity time-domain simulation tool, QBlade [11].

This paper is structured as follows: Section II describes the problem, together with all the requirements for control synthesis. Afterwards, the control design procedure is discussed in Section III. The developed controllers are then tested in a mid-fidelity simulation environment in Section IV. Finally, Section V will draw the conclusion.

II. FLOATING WIND TURBINE DESCRIPTION

In this section, the FOWT model is given, and a description of the estimation and identification procedures used to obtain the linear model used for the control design is explained.

A. Floating Wind turbine Model

For this study, the DTU 10 MW Reference Wind Turbine (RWT) [12] atop a spar floating platform [13] within the context of the SOFTWIND project [14]. The parameters of both the DTU 10 MW RWT and the floating platform are shown in Table I and Table II, respectively.

TABLE I
PARAMETERS OF THE DTU 10 MW RWT [12].

Parameter	Value
Cut-in wind speed	4 [m/s]
Cut-out wind speed	25 [m/s]
Rated wind speed	11.4 [m/s]
Rated power	10 [MW]
Peak power coefficient	0.48 [-]
Optimal tip speed ratio	7.55 [-]
Rotor diameter	178.3 [m]
Hub Height	119 [m]
Minimum rotor speed	6 [rpm]
Maximum rotor speed	9.6 [rpm]
Rotor mass	227,962 [kg]
Nacelle mass	446,036 [kg]
Tower mass	628,442 [kg]

TABLE II
PARAMETERS OF THE SOFTWIND SPAR PLATFORM [13].

Parameter	Value
Platform mass	$1.94 \times 10^7 [kg]$
Roll inertia about CoG FOWT	$10^{10} [kg.m^2]$
Pitch inertia about CoG FOWT	$10^{10} [kg.m^2]$
Yaw inertia about CoG FOWT	$6 \times 10^8 [kg.m^2]$
Draft	90 [m]
Platform diameter	18 [m]

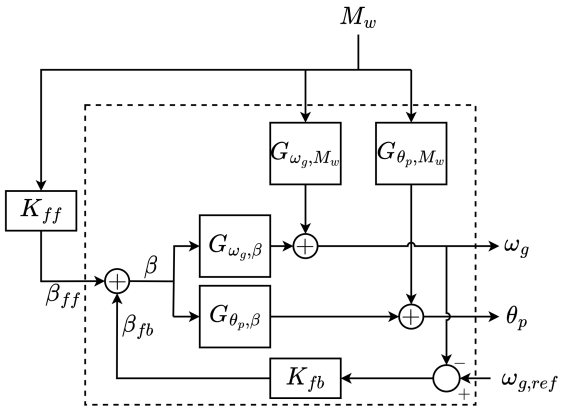

Fig. 2. Block diagram of the closed-loop floating wind turbine model, where the FB controller is embedded within the model, with the relevant blocks and signals required for the identification.

Fig. 2 shows a block diagram of the FOWT model and control signals. Each block represents a linear Transfer Function (TF). The tilting wave moments are represented by M_w. G_{θ_p,M_w} is mapping from, M_w, to the platform pitch motion, θ_p, the effect of wave moments on the generator speed, ω_g. Similar to the wave moment, the effect of blade pitch on generator speed and platform pitch motion is described by the TFs $G_{\omega_g,\beta}$ and $G_{\theta_p,\beta}$, respectively.

To obtain these TFs, which are required for the control design, identification is conducted on the results obtained from QBlade [11]. QBlade is a fully coupled, non-linear, aero-hydro-servo-elastic wind turbine simulation suite that is capable of wind turbines with a good level of accuracy. System identification is required when using QBlade for control design purposes, as it is not equipped with a linearization functionality, and thus, making it complicated to do model-based control.

B. Spectral Estimation and Identification

This work was done at an average wind speed of 16 [m/s] as an operating point. A similar procedure was used for both the the estimation, and the identification, where an experiment of duration of 25000 [s] was held in QBlade.

To get the TFs $G_{\omega_g,\beta}(s)$ and $G_{\theta_p,\beta}(s)$, a chirp signal, logarithmically distributed over the experiment's duration, was used to excite β within a frequency band (0.02 to 0.3 Hz). As for $G_{\omega_g,M_w}(s)$ and $G_{\theta_p,M_w}(s)$, a JONSWAP spectrum was used.

From input-output data, spectral estimation can be employed to get the above-mentioned TFs in a non-parametric form. A frequency response function (FRF), assuming no correlation between the input and noise signals, can be achieved according to:

$$G_{y,u}(j\omega) = \frac{S_{yu}(j\omega)}{S_{uu}(j\omega)}, \tag{1}$$

where ω in (1) denotes the frequency, $j = \sqrt{-1}$, while $S_{yu}(j\omega)$ is the cross-spectral density of the output and input, $S_{uu}(j\omega)$ is the power spectral density of the input, and $G_{y,u}(j\omega)$ represents the estimated FRF. Based on the estimated frequency response functions and the feedforward structure given in Fig. 2 the optimal non-parametric feedforward controller for generator speed control and tower top control can be estimated and are respectively given by:

$$K_{ff,\omega}(j\omega) = -\frac{G_{\omega_g,M_w}(j\omega)}{G_{\omega_g,\beta}(j\omega)}, \tag{2}$$

$$K_{ff,\theta_p}(j\omega) = -\frac{G_{\theta_p,M_w}(j\omega)}{G_{\theta_p,\beta}(j\omega)}. \tag{3}$$

The optimal non-parametric controllers are given by the blue lines in Fig. 4 and Fig. 5, respectively.

So far, the controllers given in (3) were obtained using non-parametric since FRFs were used. However, they cannot be used for control implementation. Therefore, identification using PDSID$_{opt}$ was conducted to obtain linear models, since QBlade lacks the linearization functionality as previously mentioned. More details about PDSID$_{opt}$ algorithm can be found in [10].

III. CONTROLLER DESIGN

For control design, the $\mathcal{H}_\infty$ framework is used. Therefore, first, we start by introducing the $\mathcal{H}_\infty$ problem set-up, before defining the generalized plant for the control synthesis, in addition to the performance weights required. Normally, the order of the synthesized $\mathcal{H}_\infty$ controllers is equal to that of the plant model. Subsequently, if the plant model is of a high order, the $\mathcal{H}_\infty$ would be high too, which makes its implementation complicated. Accordingly, lower-order controllers with fixed-structure are employed instead, with the $\mathcal{H}_\infty$ controllers used as reference. Finally, both the $\mathcal{H}_\infty$ and the parametric reduced-order controllers, are then compared with the non-parametric optimal FF controller obtained from the spectral estimation from II.

The objective of formulating the control problem in the $\mathcal{H}_\infty$ framework is to minimize the $\mathcal{H}_\infty$ norm of the TF from the exogenous inputs, w, to performance outputs, z [15]. The controller synthesis problem is then to find a controller K_{ff} that minimizes the infinity norm of the closed-loop TF, $||N||_\infty < 1$.

The generalized plant, P, used for the control synthesis is shown in Fig. 3. The exogenous input, w, considered is the wave moment, M_w, while two performance signals, z_1 and z_2, are specified. Signal z_1 represents the weighted response penalized by the weight W_p to reduce the effect of M_w, while z_2 is the weighted control action penalized by the weight W_u

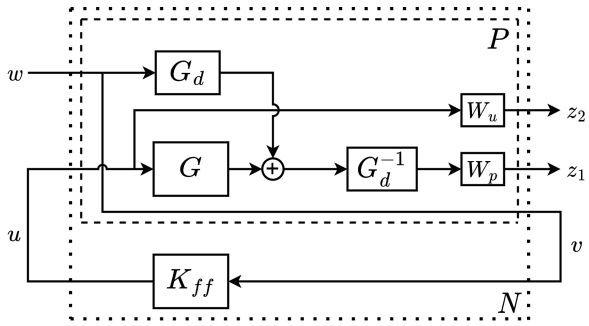

Fig. 3. Generalized plant with the performance weights

to bound the actuator limits. Signals v and u represent the control input (M_w) and the control action (β), respectively. As for G and G_d, they are defined based on the control objective. For FF-ω, $G = G_{\omega_g,\beta}$ and $G_d = G_{\omega_g,M_w}$, while for FF-θ_p, $G = G_{\theta_p,\beta}$ and $G_d = G_{\theta_p,M_w}$.

$W_p(s)$ is chosen to get a slope of 20 dB/dec in $|S|$ for the low frequency region as follows

$$W_p(s) = \frac{s/M + \omega_B}{s + A\omega_B}, \tag{4}$$

with ω_B as the desired closed-loop bandwidth, A is the desired disturbance attenuation within the closed-loop bandwidth, and M is the desired bound on the sensitivity margin [15]. The controller sensitivity is penalized at high frequencies by W_u, which was considered constant in this work.

The controller is designed that based on v, a control signal, u, is generated to counteract the influence of w, on z, by minimizing the weighted $\mathcal{H}_\infty$ norm of the closed-loop TFs, N, from w to z_1 and z_2:

$$N(s) = \begin{bmatrix} W_p\Big(I + G_d^{-1}GK_{ff}\Big) \\ W_u K_{ff} \end{bmatrix}, \tag{5}$$

where the FF controller sensitivity function is defined as:

$$S_{ff}(s) = \Big(I + G_d^{-1}GK_{ff}\Big). \tag{6}$$

S_{ff} gives an indication about the effectiveness of the FF controller can be evaluated in the frequency domain, as it shows that the undesirable effect of the exogenous input, w, altering the exogenous output, z_1, can be totally cancelled out or at least mitigated to some extent by the inclusion of the FF controller, K_{ff}, as demonstrated in (6). In theory, perfect disturbance cancellation can be achieved by substituting K_{ff} in (5) with the FF controllers in (3), N_1 becomes zero indicating that $S_{ff} = 0$, and that perfect disturbance rejection has been achieved.

$$z_{1,noFF} = G_d w \tag{7}$$

$$z_{1,FF} = W_p\left(I + G_d^{-1}GK_{ff}\right)w \tag{8}$$

$$\frac{z_{1,FF}}{z_{1,noFF}} = \frac{W_p\left(I + G_d^{-1}GK_{ff}\right)}{G_d} \tag{9}$$

Equations (7) and (8) show the disturbance signal transfer to the output signal in the absence and the presence of the FF controller, respectively, while (9) compare both responses. It can clearly be seen how K_{ff} is able to alleviate the effects of w on z_1 when that ratio in (9) is less than unity.

The wave FF controller, K_{ff}, can then be obtained via the minimization of the mixed-sensitivity problem with respect to K_{ff}:

$$\min_{\mathrm{K_{ff}}} ||N||_\infty. \tag{10}$$

Following the control synthesis, the high-order $\mathcal{H}_\infty$ controllers are reduced by fitting fixed-structure, lower-order controllers, as shown for both generator speed and platform pitch motion in Fig. 4 and Fig. 5, respectively. The parametric FF-ω controller is then given as:

$$K_{ff,\omega}(s) = \frac{K_\omega}{s^2}\frac{\tau s + 1}{s^2 + 2\zeta\omega s + \omega^2}, \tag{11}$$

while the parametric FF-θ_p controller, can either be a static gain, K_{θ_p}, or a dynamic controller expressed as:

$$K_{ff,\theta_p}(s) = \frac{K_{\theta_p} s^2}{s^2 + 2\zeta\omega s + \omega^2}, \tag{12}$$

where K_ω and K_{θ_p} are constants used for scaling the controller gain, τ is a time constant, ζ is the damping ratio, and ω is the natural frequency.

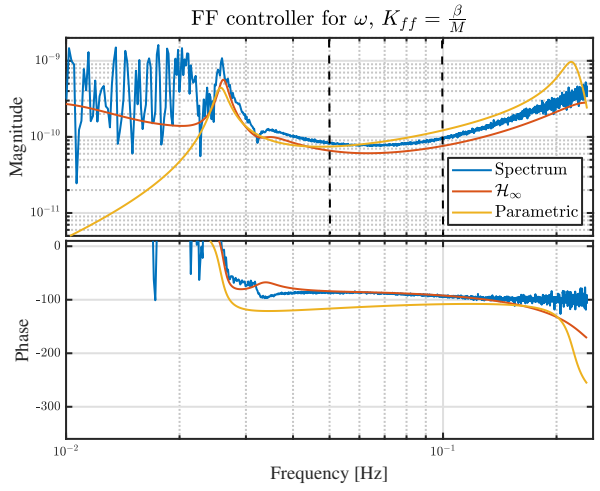

Fig. 4. Bode plot of the optimal feedforward controller that targets the high speed shaft rotor speed. Blue: spectral estimate, Red: $\mathcal{H}_\infty$ control, Yellow: parametric controller.

Investigating Fig. 4 and Fig. 5, they show a good agreement between the non-parametric optimal FF controller, and the $\mathcal{H}_\infty$ controller within the frequency band of interest enclosed by the dashed vertical lines.

Additionally, it is important to mention that the synthesized $\mathcal{H}_\infty$ controllers are, by definition, stable because the internal stability of the feedback system, with the baseline FB controller, is guaranteed. Furthermore, the $\mathcal{H}_\infty$ formulation ensures producing stable FF controllers, unlike the model-inversion FF controllers [5], [9], which would require adding extra elements to the inverted controller to make it stable, in case of non-minimum phase systems comprising RHPZs [2] inverted to become unstable poles.

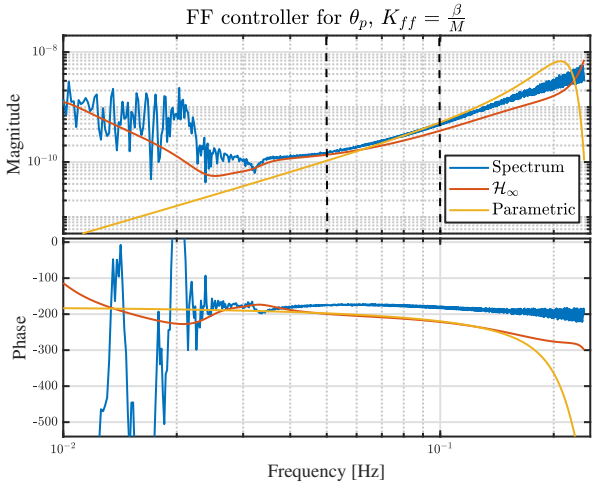

Fig. 5. Bode plot of the optimal feedforward controller that targets the platform pitch. Blue: spectral estimate, Red: $\mathcal{H}_\infty$ control, Yellow: parametric controller.

IV. RESULTS

In this section, the parametric controller is assessed in mid-fidelity time-domain simulations, using the linear models developed in Section II.

The synthesized controllers were augmented to the baseline FB controller, and their performance, under the normal operating environmental conditions of wind and waves, is compared to the normal baseline FB control. Additionally, the effect of each of the wind and waves disturbances is shown separately in the absence the other to show the frequency band where each disturbance exists. Wind disturbances are less frequent compared to wave disturbances implying that wind dominates in the low-frequency range, while its dominance diminishes as frequency increases where waves become more dominant. This observation is supported by the power spectra in Fig. 7.

The power spectral density (PSD) spotlights the frequency band ranging up to 0.3 Hz, which is the linear wave range (0.05–0.3 Hz), where the wave FF controllers are active reacting only to wave disturbance, while has no effect at lower frequencies.

The feedforward controller for rotor speed regulation (FF-ω) is designed to mitigate wave-induced variations. This is demonstrated by the FBFF-ω controller that evidently alleviates the fluctuations in the generator speed, which in return reduces the oscillations in the generator power as shown in Fig. 6. This is illustrated in the PSD in Fig. 7 where the energy content of the generator speed, as well as the power, are decreased, within the wave frequency range, below the

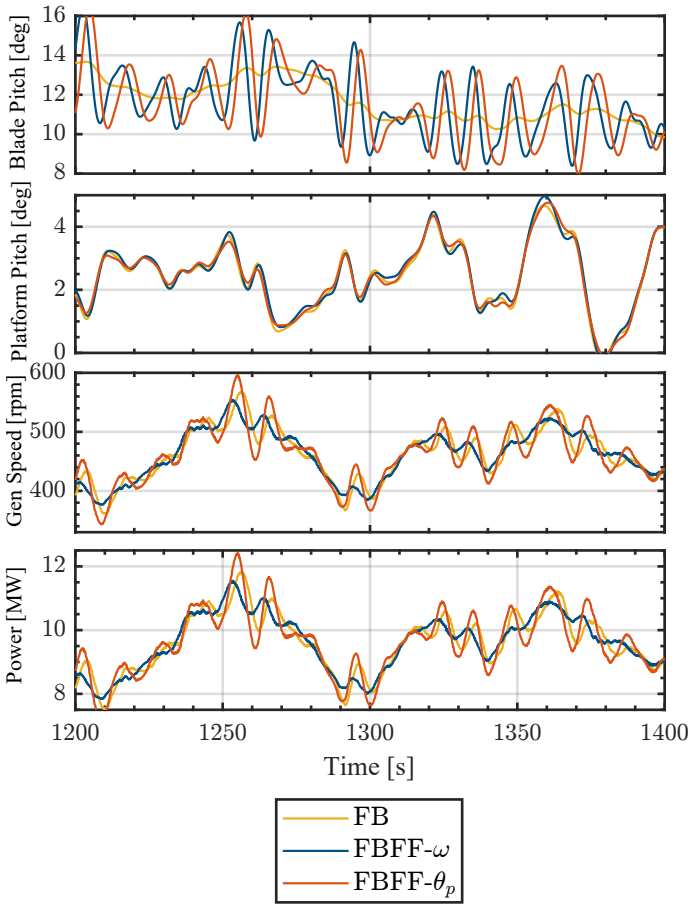

Fig. 6. Time series of the blade pitch, platform pitch, generator speed and power at 16 m/s turbulent wind.

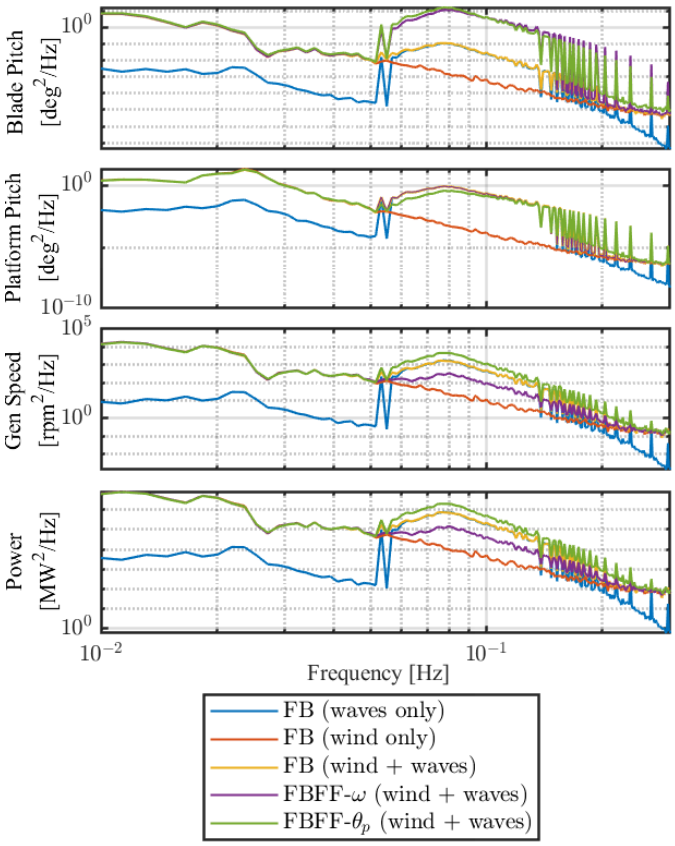

Fig. 7. Power spectral density of the blade pitch, platform pitch, generator speed and power at 16 m/s turbulent wind.

normal FB operating condition with both wind and waves. The energy content of both the blade pitch actuation and platform pitch, on the other hand, increases indicating more oscillations in these channels, which is clearly manifested in Fig. 6.

While the feedforward controller for load minimization (FF-θ_p), on the other hand, is designed to reduce the oscillations of the rigid body platform pitch motion, which is illustrated by the FBFF-θ_p controller as the addition of the FF-θ_p control to the FB control counteracts the wave-induced platform pitch motion, and slightly reduces the platform pitch motion. However, this comes at the expense of increasing the blade pitch command, rotor speed and power excursions as shown in Fig. 6. This is highlighted in the PSD in Fig. 7 where the energy content of the platform pitch is reduced, while that of the blade pitch, the generator speed and the power increased above the normal FB operating condition with both wind and waves.

Both FF controllers modify the blade pitch command to meet their control objective, which is lower fluctuations in either the rotor speed or platform pitch motion for speed regulation and load minimization, respectively. According to Fig. 6 and Fig. 7, they are opposing each other even though their respective blade pitch command is nearly the same. Yet, this opposing action is due to the phase difference between the two signals. This makes achieving both control objectives at the same time challenging.

Regarding fatigue loading, the performance of the FF controllers is assessed by means of computing the variance of some signals, while conducting damage equivalent load (DEL) analysis based on the rainflow counting technique, for others. DEL was computed for the FB with both wind and waves acting separately and combined to show the distinct effect of each of them independently, while for FBFF-ω and FBFF-θ_p, combined wind and waves scenario was considered as Fig. 8 shows. It is clear that wind contributes more to the fatigue loads than waves except for thrust force, which is reasonable since the waves cause continuous variation in the relative wind speed seen by the rotor, and thus, the rotor thrust varies as a result.

As for FF-ω, the wave FF controller reduces the rotor thrust force. Blade pitch command increases due to the extra blade pitching from the wave-FF. As a result, the rotor thrust force is decreased, leading to less DEL. The effect of the FF-ω on the platform pitch motions and the blade-out-of-plane bending fatigue damage is almost insignificant, while the blade pitch variation increases by nearly double over the normal FB case indicating more fatigue damage experienced by the pitch actuator.

Concerning FF-θ_p, the wave FF controller is very efficient

at reducing the rigid body platform pitch mode, hence, the tower-top FA motion. This curtailment in the platform pitch motion leads to a lower blade-out-of-plane bending fatigue damage, whereas the blade pitch actuator is heavily loaded even more than in the FF-ω case, which causes a significant increase in the rotor thrust. By means of linear analysis, this increase in the thrust force can be explained, as according to [16] there exists an anti-resonance peak at the platform pitch eigenfrequency in the TF from blade pitch to thrust, which a resonance peak at the same frequency in the TF from the blade pitch to the tower top FA displacement.

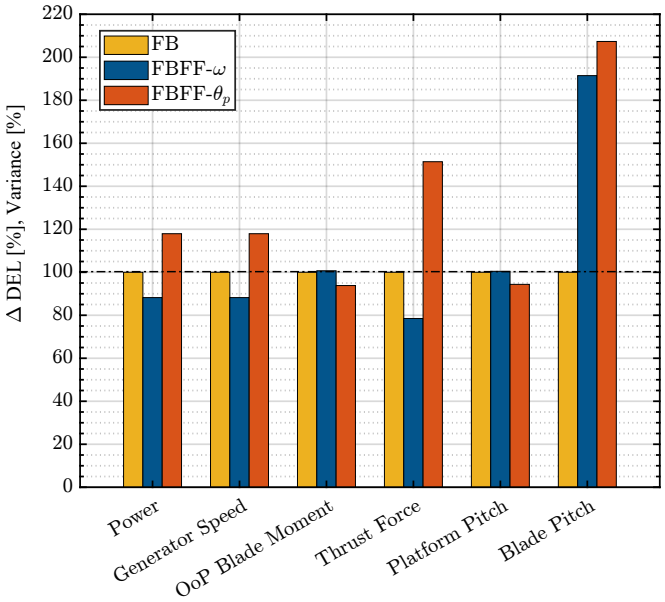

Fig. 8. Damage Equivalent Load and variance with combined feedback-feedforward compared to feedback control

V. CONCLUSIONS

In this paper, a feedforward control strategy was developed with the aim of reducing the wave disturbance on floating wind turbines. Two feedforward controllers were designed using the $\mathcal{H}_\infty$ framework; the objective of the first one was power regulation through mitigating the wave-induced generator speed fluctuations, while the objective of the second is load minimization by alleviating the platform pitch motion. To accomplish these objectives, linear models of the floating wind turbine were identified using the PBSID$_{opt}$ algorithm. Then they were implemented within a generalized plant and employed in the $\mathcal{H}_\infty$ control synthesis. Subsequently, the $\mathcal{H}_\infty$ controllers were parameterized into fixed-structure lower-order controllers. The feedforward controllers were designed for the DTU 10MW reference wind turbine on top of a spar floating platform developed within the SOFTWIND project.

Time-domain simulations were then conducted in QBlade to evaluate the feedforward control strategy benefits in terms of structural loads and power quality for the floating wind turbine components. It was found that the feedforward controller for rotor speed reduces the power fluctuations, while the one for platform pitch motion reduces the OoP blade loads associated with wave excitation. The proposed feedforward control strategy does not require modifying the industry-standard feedback controller. It requires a forecast of the incoming waves, which is feasible to get with technologies that are already used in the maritime industry, and this is to be integrated into the wind turbine control system.

REFERENCES

[1] European Commission, "EU renewable energy targets." (accessed: 05-02-2023). [Online]. Available: https://energy.ec.europa.eu/topics/renewable-energy/renewable-energy-directive-targets-and-rules/renewable-energy-targets_en

[2] A. Hegazy, P. Naaijen, and J. W. van Wingerden, "A novel control architecture for floating offshore wind turbines," in *IFAC 22nd World Congress*, 2023.

[3] D. Schlipf, D. J. Schlipf, and M. Kühn, "Nonlinear model predictive control of wind turbines using lidar," *Wind Energy*, vol. 16, no. 7, pp. 1107–1129, 2013.

[4] S. T. Navalkar, J. W. van Wingerden, P. A. Fleming, and G. Van Kuik, "Integrating robust lidar-based feedforward with feedback control to enhance speed regulation of floating wind turbines," in *2015 American Control Conference (ACC)*. IEEE, 2015, pp. 3070–3075.

[5] A. Fontanella, M. Al, J. van Wingerden, and M. Belloli, "Model-based design of a wave-feedforward control strategy in floating wind turbines," *Wind Energy Science*, vol. 6, no. 3, pp. 885–901, 2021.

[6] P. Naaijen and A. P. Wijaya, "Phase Resolved Wave Prediction From Synthetic Radar Images," ser. International Conference on Offshore Mechanics and Arctic Engineering, vol. Volume 8A: Ocean Engineering, 2014.

[7] S. Raach, D. Schlipf, F. Sandner, D. Matha, and P. W. Cheng, "Nonlinear model predictive control of floating wind turbines with individual pitch control," in *2014 American Control Conference*, 2014, pp. 4434–4439.

[8] Y. Ma, P. D. Sclavounos, J. Cross-Whiter, and D. Arora, "Wave forecast and its application to the optimal control of offshore floating wind turbine for load mitigation," *Renewable Energy*, vol. 128, pp. 163–176, 2018.

[9] M. Al, A. Fontanella, D. van der Hoek, Y. Liu, M. Belloli, and J. W. van Wingerden, "Feedforward control for wave disturbance rejection on floating offshore wind turbines," in *Journal of Physics: Conference Series*, vol. 1618, no. 2. IOP Publishing, 2020, p. 022048.

[10] G. van der Veen, J. W. van Wingerden, M. Bergamasco, M. Lovera, and M. Verhaegen, "Closed-loop subspace identification methods: an overview," *IET Control Theory & Applications*, vol. 7, no. 10, pp. 1339–1358, 2013.

[11] D. Marten, "Qblade Website," (accessed: 02-02-2023). [Online]. Available: http://www.q-blade.org

[12] C. Bak, F. Zahle, R. Bitsche, T. Kim, A. Yde, L. C. Henriksen, M. H. Hansen, J. P. A. A. Blasques, M. Gaunaa, and A. Natarajan, "The dtu 10-mw reference wind turbine," in *Danish wind power research 2013*, 2013.

[13] V. Arnal, "Modélisation expérimentale d'une éolienne flottante par une approche sofware-in-the-loop," Ph.D. dissertation, 2020. [Online]. Available: http://www.theses.fr/2020ECDN0037

[14] "SOFTWIND," (accessed: 02-02-2023). [Online]. Available: https://www.weamec.fr/en/projects/softwind

[15] S. Skogestad and I. Postlethwaite, *Multivariable Feedback Control: Analysis and Design*. John Wiley & Sons, 2007.

[16] D. van den Berg, D. de Tavernier, and J. W. van Wingerden, "The dynamic coupling between the pulse wake mixing strategy and floating wind turbines," *Wind Energy Science*, vol. 8, no. 5, pp. 849–864, 2023.